Charge Redistribution in Oxidized and Semiquinone E. coli DNA Photolyase upon Photoexcitation: Stark Spectroscopy Reveals a Rationale for the Position of Trp382

3 AUTHORS:

Goutham Kodali
University of Pennsylvania
30 PUBLICATIONS   152 CITATIONS

SEE PROFILE

Umar Salim
Universitas Mulawarman
1 PUBLICATION   20 CITATIONS

SEE PROFILE

Robert J Stanley
Temple University
47 PUBLICATIONS   963 CITATIONS

SEE PROFILE

Charge Redistribution in Oxidized and Semiquinone *E. coli* DNA Photolyase upon Photoexcitation: Stark Spectroscopy Reveals a Rationale for the Position of Trp382

Goutham Kodali,[†] Salim U. Siddiqui,[‡] and Robert J. Stanley*,[†]

Department of Chemistry, Temple University, Philadelphia, Pennsylvania 19122, and Department of Radiation Oncology, Henry Ford Hospital, Detroit, Michigan 48202

Received November 25, 2008; E-mail: rstanley@temple.edu

Abstract: The electronic structure of the two lowest excited electronic states of FAD and FADH• in folate-depleted *E. coli* DNA photolyase (PL$_{OX}$ and PL$_{SQ}$, respectively) was measured using absorption Stark spectroscopy. The experimental analysis was supported by TDDFT calculations of both the charge redistribution and the difference dipole moments for the transitions of both oxidation states using lumiflavin as a model. The difference dipole moments and polarizabilities for PL$_{OX}$ are similar to those obtained in our previous work for flavins in simple solvents and in an FMN-containing flavoprotein. No such comparison can be made for PL$_{SQ}$, as we believe this to be the first experimental report of the direction and magnitude of excited-state charge redistribution in any flavosemiquinone. The picture that emerges from these studies is discussed in the context of electron transfer in photolyase, particularly for the semiquinone photoreduction process, which involves nearby tryptophan residues as electron donors. The direction of charge displacement derived from an analysis of the Stark spectra rationalizes the positioning of the critical Trp382 residue relative to the flavin for efficient vectorial electron transfer leading to photoreduction. The ramifications of vectorial charge redistribution are discussed in the context of the wider class of flavoprotein blue light photoreceptors.

Introduction

DNA photolyase is a light-driven flavoprotein that repairs cyclobutylpyrimidine dimers (CPDs) in UV-damaged DNA.[1,2] The protein is found in all kingdoms, including nonplacental mammals. Two noncovalently bound cofactors are associated with PL. One is an absolutely conserved flavin adenine dinucleotide (FAD) molecule without which the protein cannot bind or repair substrate. The second cofactor appears to function as a photoantenna, although the protein can bind and repair DNA without it.

Photolyase binds to the CPD in a light-independent manner. Substrate binding does not depend to any significant degree on the oxidation state of the flavin.[3,4] The earliest crystal structure of photolyase revealed a surface-accessible cavity with the approximate dimensions of a CPD, and it was suggested that base flipping of the CPD was required to bring the substrate close to the flavin cofactor found at the base of this cavity.[5] This base flipping hypothesis, tested by several indirect means,[6–8]

was ultimately confirmed by a crystal structure of PL with a modified substrate molecule.[9]

The FAD must be fully reduced (FADH⁻, PL$_{RED}$) for repair to take place, and we[10] and others[11–14] have shown that direct excitation of the FADH⁻ cofactor leads to efficient CPD repair through ultrafast electron transfer from *FADH⁻ to an as yet unknown initial acceptor. Ultimately, the radical anion of the dimer, CPD•⁻, is formed, although definitive evidence for this intermediate is still lacking, and the flavin becomes oxidized to FADH•. FADH• is therefore an intermediate in the electron transfer pathway. At some point in the reaction cycle, the CPD•⁻ undergoes a thermally activated monomerization reaction[15,16] to yield a thymine and thymine radical anion, T⁻•. Back electron transfer from FADH•−T⁻•→FADH⁻−T brings the flavin back

[†] Temple University.

[‡] Henry Ford Hospital.

(1) Kay, C. W. M.; Bacher, A.; Fischer, M.; Richter, G.; Schleicher, E.; Weber, S. *Compr. Ser. Photochem. Photobiol. Sci.* **2006**, *6*, 151–182.

(2) Sancar, A. *Chem. Rev.* **2003**, *103*, 2203–2237.

(3) Sancar, G. B.; Jorns, M. S.; Payne, G.; Fluke, D. J.; Rupert, C. S.; Sancar, A., III. *J. Biol. Chem.* **1987**, *262*, 492–8.

(4) Jorns, M. S.; Sancar, G. B.; Sancar, A. *Biochemistry* **1985**, *24*, 1856–61.

(5) Park, H.-W.; Kim, S.-T.; Sancar, A.; Deisenhofer, J. *Science* **1995**, *268*, 1866–72.

(6) Berg, B. J. V.; Sancar, G. B. *J. Biol. Chem.* **1998**, *273*, 20276–20284.

(7) Butenandt, J.; Burgdorf, L. T.; Carell, T. *Angew. Chem., Int. Ed.* **1999**, *38*, 708–711.

(8) Christine, K. S.; MacFarlane, A. W., IV; Yang, K.; Stanley, R. J. *J. Biol. Chem.* **2002**, *277*, 38339–38344.

(9) Mees, A.; Klar, T.; Gnau, P.; Hennecke, U.; Eker, A. P. M.; Carell, T.; Essen, L.-O. *Science* **2004**, *306*, 1789–1793.

(10) MacFarlane, A. W., IV; Stanley, R. J. *Biochemistry* **2003**, *42*, 8558–8568.

(11) Kao, Y.-T.; Saxena, C.; Wang, L.; Sancar, A.; Zhong, D. *Proc. Natl. Acad. Sci. U.S.A.* **2005**, *102*, 16128–16132.

(12) Langenbacher, T.; Zhao, X.; Bieser, G.; Heelis, P. F.; Sancar, A.; Michel-Beyerle, M. E. *J. Am. Chem. Soc.* **1997**, *119*, 10532–10536.

(13) Kim, S.-T.; Volk, M.; Rousseau, G.; Heelis, P. F.; Sancar, A.; Michel-Beyerle, M.-E. *J. Am. Chem. Soc.* **1994**, *116*, 3115–16.

(14) Okamura, T.; Sancar, A.; Heelis, P. F.; Begley, T. P.; Hirata, Y.; Mataga, N. *J. Am. Chem. Soc.* **1991**, *113*, 3143–5.

(15) Yeh, S. R.; Falvey, D. E. *J. Am. Chem. Soc.* **1991**, *113*, 8557–8.

(16) Austin, R.; McMordie, S.; Altmann, E.; Begley, T. P. *J. Am. Chem. Soc.* **1993**, *115*, 10370–1.
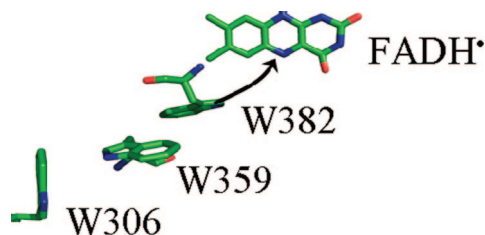
Figure 1. The spatial arrangement of the FADH⁻ acceptor with the Trp donor residues that facilitate photoreduction in *E. coli* photolyase, taken from Kim et al. (PDB entry 1DNP[5]). The arrow indicates the direction of the initial electron transfer following photoexcitation of FADH⁻. The N atom on W382 is about 5.7 Å from N₅ on the flavin.

to the fully reduced form in the ground state. Product release subsequently occurs, but little is known about this process.

The second chromophore appears to function as a light harvesting antenna.[17] The identity of the second cofactor depends on the organism. In *E. coli* PL folate is found,[18] but it is deazaflavin in *A. nidulans*.[19] Apparently FAD is also used as the chromophore, as has been observed for *S. tokodaii*.[20] In earlier studies, it was concluded that the function of this secondary chromophore was to facilitate the photoreduction of FADH⁻ to FADH⁻.[21] The reduced flavin is stable if an exogenous electron donor is available to reduce the terminal Trp residue. It was thought that this photoreduction reaction was a physiologically relevant process, based on the observation that the in vitro purified protein was in the semiquinone form. However, more recent studies suggest that PL is probably fully reduced in the cell, and therefore photoreduction does not appear to be tied to DNA repair.[22]

Efforts by several groups have shown that the photoreduction of FADH⁻ involves a set of highly conserved tryptophan (Trp) residues in *E. coli* PL.[23,24] In fact, *E. coli* PL has 15 Trp residues, a large number for a protein with 471 amino acids. W382 is less than 6 Å from the flavin N₅ atom and is located under the flavin below the xylene ring (see Figure 1; a numbering scheme for the flavin ring system can be seen in Figure 3a). In *E. coli* PL, photoexcitation of FADH⁻ leads to ultrafast electron abstraction from W382, which, in turn, pulls an electron from W359.[25] The electron transfer chain terminates when the cation radical of W306, formed by electron transfer to W359•⁺, is reduced by an exogenous donor. Of the other 12 Trp residues, W277 is known to be critical in substrate binding and may be involved in the DNA repair reaction directly.[26]

One is led to wonder why the Trp triad involved in photoreduction is located where it is. Are there electronic
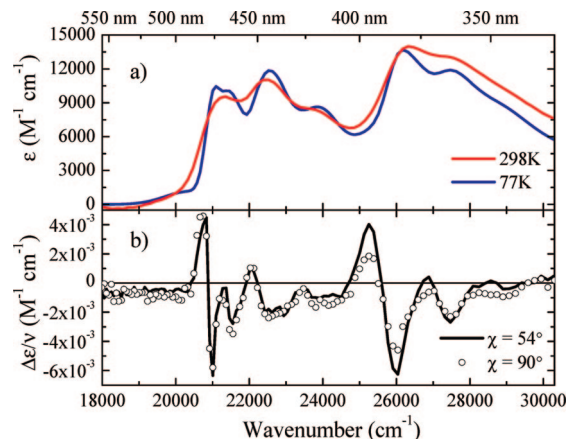

Figure 2. (a) Room temperature (red line, 21 μM) and 77 K (blue line, 21 μM) absorption spectra of PL$_{OX}$ in glycerol:buffer. (b) Energy-weighted Stark spectra of 220 μM PL$_{OX}$ at $\chi = 54°$ (−) and 90° (○), normalized to 1 MV/cm. The symbol used to plot the 90° data is sized to appropriately reflect the magnitude of the standard deviation from the mean for the averaged scans.

characteristics of the FADH⁻ excited state that require that W382 be proximal to the xylene ring? Why is W382 underneath C₆ as opposed to above C₉, or N₁, C₄, etc.? Knowledge of the charge distribution of the excited states of FADH⁻ is central to answering these questions. Another issue is whether photoreduction of the oxidized form of the protein[27] proceeds in a similar fashion.

These issues take on greater significance in studies of cryptochromes (Cry),[1,2,28,29] PL homologues that have no DNA repair activity but act as blue light photoreceptors (with the exception of the Cry-DASH protein, which has been shown to act as a single-strand CPD photolyase[30,31]). Cry has both the required FAD and a second chromophore. However, it is often very difficult to photoreduce FADH⁻ in Cry.[32,33] Furthermore, there is speculation that this blue light photoreceptor may utilize the flavin radical, at least in avian Cry, so as to visualize the Earth's magnetic field to the avian eye for migratory purposes.[34−38]

While PL$_{OX}$ has not been shown to have a physiological function (but see below), there are photoactive flavoproteins that use oxidized flavin, FAD or flavin mononucleotide (FMN), in blue light signal transduction.[29] These include the LOV and BLUF domain proteins. FMN-containing LOV domains,[39]

(17) Jorns, M. S.; Sancar, G. B.; Sancar, A. *Biochemistry* **1984**, *23*, 2673–9.
(18) Johnson, J. L.; Hamm-Alvarez, S.; Payne, G.; Sancar, G. B.; Rajagopalan, K. V.; Sancar, A. *Proc. Natl. Acad. Sci. U.S.A.* **1988**, *85*, 2046–50.
(19) Tamada, T.; Kitadokoro, K.; Higuchi, Y.; Inaka, K.; Yasui, A.; De Ruiter, P. E.; Eker, A. P. M.; Miki, K. *Nat. Struct. Biol.* **1997**, *4*, 887–891.
(20) Fujihashi, M.; Numoto, N.; Kobayashi, Y.; Mizushima, A.; Tsujimura, M.; Nakamura, A.; Kawarabayasi, Y.; Miki, K. *J. Mol. Biol.* **2007**, *365*, 903–910.
(21) Hamm-Alvarez, S.; Sancar, A.; Rajagopalan, K. V. *J. Biol. Chem.* **1990**, *265*, 18656–62.
(22) Kavakli, I. H.; Sancar, A. *Biochemistry* **2004**, *43*, 15103–15110.
(23) Li, Y. F.; Heelis, P. F.; Sancar, A. *Biochemistry* **1991**, *30*, 6322–9.
(24) Aubert, C.; Mathis, P.; Eker, A. P.; Brettel, K. *Proc. Natl. Acad. Sci. U.S.A.* **1999**, *96*, 5423–7.
(25) Aubert, C.; Vos, M. H.; Mathis, P.; Eker, A. P. M.; Brettel, K. *Nature* **2000**, *405*, 586–590.
(26) Li, Y. F.; Sancar, A. *Biochemistry* **1990**, *29*, 5698–706.

(27) Jorns, M. S.; Baldwin, E. T.; Sancar, G. B.; Sancar, A. *J. Biol. Chem.* **1987**, *262*, 486–91.
(28) Partch, C. L.; Sancar, A. *Photochem. Photobiol.* **2005**, *81*, 1291–1304.
(29) Losi, A. *Photochem. Photobiol.* **2007**, *83*, 1283–1300.
(30) Huang, Y.; Baxter, R.; Smith, B. S.; Partch, C. L.; Colbert, C. L.; Deisenhofer, J. *Proc. Natl. Acad. Sci. U.S.A.* **2006**, *103*, 17701–17706.
(31) Selby, C. P.; Sancar, A. *Proc. Natl. Acad. Sci. U.S.A.* **2006**, *103*, 17696–17700.
(32) Cashmore, A. R.; Jarillo, J. A.; Wu, Y.-J.; Liu, D. *Science* **1999**, *284*, 760–765.
(33) Bouly, J.-P.; Schleicher, E.; Dionisio-Sese, M.; Vandenbussche, F.; Van Der Straeten, D.; Bakrim, N.; Meier, S.; Batschauer, A.; Galland, P.; Bittl, R.; Ahmad, M. *J. Biol. Chem.* **2007**, *282*, 9383–9391.
(34) Wiltschko, R.; Wiltschko, W. *BioEssays* **2006**, *28*, 157–168.
(35) Mouritsen, H.; Ritz, T. *Curr. Opin. Neurobiol.* **2005**, *15*, 406–414.
(36) Solov'yov, I. A.; Chandler, D. E.; Schulten, K. *Biophys. J.* **2007**, *92*, 2711–2726.
(37) Ritz, T.; Adem, S.; Schulten, K. *Biophys. J.* **2000**, *78*, 707–718.
(38) Gegear, R. J.; Casselman, A.; Waddell, S.; Reppert, S. M. *Nature* **2008**, *454*, 1014–1018.
(39) Kennis, J. T. M.; Alexandre, M. T. A. *Compr. Ser. Photochem. Photobiol. Sci.* **2006**, *6*, 287–319.

including phototropins,[40] are responsible for a wide variety of blue light responses in bacteria, plants, and animals. Blue light excitation of the FMN leads to reasonably efficient singlet to triplet intersystem crossing (^{1}FMN$\rightarrow$^{3}FMN). The triplet flavin then forms a cysteinyl adduct with a highly conserved cysteine residue positioned close to the C_{4a} of the flavin. BLUF (blue light using FAD) proteins are involved in the photoregulation of photosynthesis.[41] This photobiological mechanism has been the subject of intense study lately. The signaling mechanism appears to involve a hydrogen-bonding alteration that engenders a conformational change.[42−44] This condition is set up by photoinduced electron transfer to the excited-state singlet of the flavin from a nearby conserved tyrosine residue to produce the Tyr$^\bullet$−FADH$^\bullet$ radical pair. The relevance of the BLUF mechanism to this study is given below.

In all of these cases, function depends on a light-induced charge redistribution of the flavin molecule, which can alter the reduction potential of the excited state relative to the ground state.[29] There have been computational studies to examine the excited state (see Discussion), but the size and asymmetry of the flavin molecule make accurate calculations difficult. Measuring the degree and direction of charge redistribution is challenging experimentally as well. However, Stark spectroscopy is one of the most powerful tools we have to elucidate the excited-state structure of flavins in various oxidation states, and we have explored charge redistribution in oxidized flavins in simple solvents[45,46] and in flavoproteins.[47] Here, we have applied absorption Stark spectroscopy, supported by time-dependent density functional theory (TDDFT) calculations, to study folate-depleted fully oxidized photolyase (PL$_{OX}$) and one electron reduced photolyase (PL$_{SQ}$). In both cases, an analysis of the Stark spectrum for the lowest excited state suggests that electron density moves toward the pyrimidine ring, leaving the xylene ring relatively electropositive. This charge redistribution is discussed in the context of PL function and the function of other photoactive flavoproteins.

Materials and Methods

Protein Purification and Photodecomposition of MTHF. The purification[48] and photodecomposition of *E. coli* PL[49] has been described previously. The purity of DNA photolyase was analyzed by SDS-PAGE and UV−vis absorption spectroscopy. The purified protein contained the two expected chromophores, FADH$^\bullet$ and MTHF. PL$_{OX}$ was obtained by removing both the FAD and the folate cofactors and then reconstituting the apoprotein with FAD$_{OX}$ only.[48]

Antenna-free PL was obtained by photodecomposing the folate so that only the flavin cofactor remained.[49] The protein was placed in a 1 cm × 1 cm quartz cuvette with a sealed cap and suspended in a 100 mL beaker half-filled with water-ice. The beaker was placed in front of a focused 150 W xenon arc lamp whose light was filtered using a long pass filter with 50% transmission above 370 nm. The sample was irradiated for 5 min, and the decrease in the folate absorbance at ∼380 nm was monitored using an HP8452A diode array spectrophotometer. This procedure was repeated approximately 4−5 times until there was no further decrease in the 380 nm absorption, indicating that MTHF photodecomposition was complete. As a final check, MTHF fluorescence was measured to ensure that PL was MTHF-free. At the end of this protocol, the protein was in the semiquinone state, but trace amounts of PL$_{OX}$ (<5%) were observed. The MTHF-depleted protein was concentrated using 30 kD MWCO centrifugal concentrators. Glycerol was added to the concentrated photolyase to a final concentration of 50% (v:v), and the protein was stored at −80 °C for further use.

Stark Spectroscopy. The basic setup of the spectrometer is the same as described previously with minor changes.[50] The H.S. Martin optical dewar was replaced with a cryogenic dual reservoir nitrogen optical dewar (JANIS Research).[51] Briefly, the Stark spectrometer consists of a 150 W Xe arc lamp focused using a fused silica lens and filtered through a 1/8 m monochromator. The filtered light was passed through a depolarizer and then polarized with a Glan−Taylor polarizer and imaged onto the sample cuvette. Transmitted light was focused onto a UV-enhanced silicon photodiode whose output was amplified using a Ketheley current preamplifier.

The sample cuvette consists of two 1" × 1" × 1.2 mm thick glass slides coated on one side with indium tin oxide (ITO, 100 Ω/cm). The ITO coatings were arranged facing each other, separated by a 55 μm kapton spacer. About 15 μL of 330 μM PL$_{SQ}$ in glycerol/buffer solution (2:1 v:v) was sandwiched between the two transparent electrodes, and the cuvette was mounted onto the cryostat sample holder using spring clips and plunged into the liquid N$_2$. The angle between the incoming light and the sample normal (parallel to the direction of the applied field) was set by rotation.

Stark spectra were obtained by scanning the probe light in equal increment energy units, typically about 77 cm^{-1} per step. This energy step at 400 nm corresponds to $\Delta\lambda = 1.4$ nm and at 700 nm $\Delta\lambda = 3.8$ nm (the 0.6 mm slits used for these scans produce a band-pass of 2 nm). A 217 Hz AC external electric field, F_{ext}, was derived from a high voltage power supply (Joe Rolfe Associates). Phase sensitive detection of change in the light intensity (ΔI) as a function of the applied external field was performed using a digital lock-in amplifier (SR830). Each collected spectrum consists of the average of nine scans taken with a 1 s time constant. These spectra were obtained at several fields and at least two different angles of χ. Six data sets were obtained for each angle of χ, and each set of data was individually fitted.

An analysis of the Stark spectra requires a high-quality low temperature absorption spectrum. We used our recently developed COWS (cryogenic optical waveguide spectrometer) technique[52] to obtain these spectra using a 5.8 cm path length in a liquid waveguide at 77 K. Room temperature absorption spectra were obtained using an HP H8452A diode array spectrometer with a 2 nm band-pass.

Liptay's Formalism of Electroabsorption. The analysis of the Stark spectra derives from Liptay.[53] The field-induced change in the extinction coefficient can be fitted to the derivatives of the zero field absorption spectrum. The energy-weighted field-induced

(40) Briggs, W. R.; Tseng, T.-S.; Cho, H.-Y.; Swartz, T. E.; Sullivan, S.; Bogomolni, R. A.; Kaiserli, E.; Christie, J. M. *J. Integr. Plant Biol.* **2007**, *49*, 4–10.
(41) Masuda, S.; Bauer, C. E. *Handb. Photosensory Receptors* **2005**, 433–445.
(42) Zirak, P.; Penzkofer, A.; Hegemann, P.; Mathes, T. *Chem. Phys.* **2007**, *335*, 15–27.
(43) Masuda, S.; Tomida, Y.; Ohta, H.; Takamiya, K.-I. *J. Mol. Biol.* **2007**, *368*, 1223–1230.
(44) Bonetti, C.; Mathes, T.; van Stokkum, I. H. M.; Mullen, K. M.; Groot, M.-L.; van Grondelle, R.; Hegemann, P.; Kennis, J. T. M. *Biophys. J.* **2008**, *95*, 4790–4802.
(45) Stanley, R. J.; Jang, H. *J. Phys. Chem. A* **1999**, *103*, 8976–8984.
(46) Stanley, R. J.; Siddiqui, M. S. *J. Phys. Chem. A* **2001**, *105*, 11001–11008.
(47) Hopkins, N.; Stanley, R. J. *Biochemistry* **2003**, *42*, 991–999.
(48) Yang, K.; Stanley, R. J. *Biochemistry* **2006**, *45*, 11239–11245.
(49) Heelis, P. F.; Payne, G.; Sancar, A. *Biochemistry* **1987**, *26*, 4634–40.
(50) Kodali, G.; Kistler, K. A.; Matsika, S.; Stanley, R. J. *J. Phys. Chem. B* **2008**, *112*, 1789–1795.
(51) Andrews, S. S.; Boxer, S. G. *Rev. Sci. Instrum.* **2000**, *71*, 3567–3569.
(52) Siddiqui, M. S. U.; Stanley, R. J. *Anal. Biochem.* **2005**, *337*, 121–129.
(53) Liptay, W. Dipole Moments and Polarizabilities of Molecules in Excited Electronic States. In *Excited States*; Lim, E. C., Ed.; Academic Press, Inc.: New York, 1974; Vol. 1, pp 129−229.

change in the extinction can be given as eq 1:

$$\frac{\Delta\varepsilon}{\bar{\nu}} = (f\,\vec{F}_{\text{ext}})^2\left\{A_\chi\frac{\varepsilon(\bar{\nu})}{\bar{\nu}} + \frac{B_\chi}{15ch}\frac{\mathrm{d}\left(\frac{\varepsilon(\bar{\nu})}{\bar{\nu}}\right)}{\mathrm{d}\bar{\nu}} + \frac{C_\chi}{30c^2h^2}\frac{\mathrm{d}^2\left(\frac{\varepsilon(\bar{\nu})}{\bar{\nu}}\right)}{\mathrm{d}\bar{\nu}^2}\right\}$$
(1)

The term $\varepsilon(\bar{\nu})$ represents the energy-weighted unperturbed absorption spectrum. $\vec{F}_{\text{ext}}$ represents the externally applied electric field, and f indicates the field correction factor for the protein core, which is related to its dielectric properties. The field correction factor is usually between 1 and 2, but is difficult to estimate especially for nonhomogeneous media like proteins.[54] The angle χ is the angle between the direction of the electric field vector of the linearly polarized probe light and the applied electric field. All of the Stark experiments reported here are performed with $\chi = 54.7°$ (magic angle) or $\chi = 90°$, after correcting for the refractive index of liquid nitrogen.

The scaling factors A_χ, B_χ, and C_χ are related to the intrinsic electronic properties of the chromophore. The A_χ term is related to the change in the transition state polarizability, and also reflects the transition hyperpolarizability, or the influence of the electric field on the transition moment. In simple terms, A_χ reflects the orientation of molecule possessing a ground-state dipole moment due to F_{ext}. Working in frozen samples restricts any response to this field, so $A_\chi \approx 0$.

Information about the change in polarizability and change in permanent dipole moment can be obtained from the B_χ and C_χ coefficients:

$$B_\chi \approx \frac{5}{2}Tr\Delta\bar{\bar{\alpha}} + (3\cos^2\chi - 1)\left(\frac{3}{2}m{\cdot}\Delta\bar{\bar{\alpha}}{\cdot}m - \frac{1}{2}Tr\Delta\bar{\bar{\alpha}}\right)$$
(2)

and

$$C_\chi = |\Delta\vec{\mu}|^2\{5 + (3\cos^2\chi - 1)(3\cos^2\zeta_A - 1)\}$$
(3)

where ζ_A is the angle between $\Delta\vec{\mu}$ and the transition dipole moment, $\vec{m}$. Here, $|\Delta\vec{\mu}|$ is the magnitude of the difference in the permanent dipole moments of the states coupled by the transition. $\Delta\bar{\bar{\alpha}}$ is the difference polarizability tensor, but we consider only the trace of the polarizability tensor, $Tr\Delta\bar{\bar{\alpha}}$, which is a scalar. The trace of a tensor is invariant with the coordinate system, so the $Tr\Delta\bar{\bar{\alpha}}$ is a good estimate of the change in the mean polarizability. When $\chi = 54.7°$, eqs 2 and 3 simplify, and the dependence on χ vanishes so that $Tr\Delta\bar{\bar{\alpha}}$ and $|\Delta\vec{\mu}|$ can be directly obtained.

From eq 1, it can be seen that the scaling parameters can be obtained by fitting the Stark spectra to the zeroth, first, and second derivatives of the absorption spectrum. This process begins by fitting the low temperature absorption spectrum to Gaussian functions. This procedure not only provides the (analytic) derivatives of the absorption spectrum, but also reduces noise that would result from a numerical differentiation of the experimental absorption spectrum. Our approach involves partitioning the absorption spectrum into two separate sets of Gaussians, each set corresponding to one of two different transitions.[46] An in-house written MATLAB routine allows for the two sets of Gaussian functions to overlap if necessary, so that distinct vibronic progressions for each transition can be included. However, we make no claim that this is a deconvolution of the spectrum, and this fit is merely a starting point for the simultaneous fitting of both the absorption and the Stark spectra.

The absorption and Stark spectra were then fitted simultaneously, with approximately equal weighting, giving two sets of A_χ, B_χ, and C_χ values. For excited states $n = 1, 2, 3...$, all reported values of $|\Delta\vec{\mu}_{0n}|$ and $Tr\Delta\bar{\bar{\alpha}}_{0n}$ are in terms of D/f and Å³/f² respectively, where

1 D = 1 debye = 3.36×10^{-30} C m and 1 Å³ = 1.113×10^{-40} C m² V⁻¹. Even though the absolute difference dipole moment and difference polarizability values depend on f, which can be difficult to calculate accurately, this uncertainty cancels when taking ratios of $|\Delta\vec{\mu}_{0n}|$, $n = 1,2$, as required below. However, this factor is required when calculating the absolute value of the shifts. In this case, an elliptical cavity approximation for f was used (see eqs 5,6 in ref 46).

TDDFT Calculations. All of the calculations were done using Gaussian 03.[55] Lumiflavin (Lf, 7,8,10-trimethyl-isoalloxazine) was used as a model flavin system. The starting geometry for Lf was taken from the isoalloxazine moiety of the (presumably) FADH• cofactor of *A. nidulans* PL,[9] in which the ribityl/adenosine moiety at N_{10} was replaced by a methyl group and hydrogen atoms were added. The geometry optimization and transition dipole moment calculations were done at the B3LYP/6-311+G (d,p)[56,57] and UB3LYP/6-311+G (d,p) levels for Lf_{OX} and Lf_{SQ}, respectively. Ten excited states were included in all excited-state calculations. However, calculations using only three excited states gave the same electronic properties as those for 10 states.

Calculations were performed for vacuum and for a polar solvent using a polarization continuum model[58] (PCM). Chloroform (CCl_4) and methanol (MeOH) were used as solvents, with dielectric constants of about 5 and 33, respectively. Difference dipole moments, $\Delta\vec{\mu}_{0n}$, were calculated using the finite field hexapole method using an external electric field of 0.001 au propagating along the $\pm x$, $\pm y$, and $\pm z$ directions in the center of mass coordinates.[59,60] The difference electron density was calculated by subtracting the SCF ground-state density from 1-particle Rho-density for the corresponding excited states.[61] Chemcraft (http://www.chemcraft-prog.com) was used to generate and visualize the excited-state dipole moment vectors and difference density figures.

Results

Low Temperature Absorption and Stark Spectra of PL_{OX}. The room and low temperature spectra of *E. coli* PL_{OX} in glycerol buffer (2:1 v:v) from 300−556 nm are shown in Figure 2a. Both spectra were obtained using our COWS spectrometer.[52] The room temperature spectrum, 21 μM in PL_{OX}, shows well-resolved vibronic structure, indicating that the cofactor is bound with minimal conformational freedom and through specific interactions. The 77 K spectrum (21 μM in PL_{OX}) shows significantly enhanced vibronic structure, with the lowest

(54) Bublitz, G. U.; Boxer, S. G. *Annu. Rev. Phys. Chem.* **1997**, *48*, 213–242.

(55) Frisch, M. J.; Schlegel, H. B.; Scuseria, G. E.; Robb, M. A.; Cheeseman, J. R.; Montgomery, J. A., Jr.; Vreven, T.; Kudin, K. N.; Burant, J. C.; Millam, J. M.; Iyengar, S. S.; Tomasi, J.; Barone, V.; Mennucci, B.; Cossi, M.; Scalmani, G.; Rega, N.; Petersson, G. A.; Nakatsuji, H.; Hada, M.; Ehara, M.; Toyota, K.; Fukuda, R.; Hasegawa, J.; Ishida, M.; Nakajima, T.; Honda, Y.; Kitao, O.; Nakai, H.; Klene, M.; Li, X.; Knox, J. E.; Hratchian, H. P.; Cross, J. B.; Bakken, V.; Adamo, C.; Jaramillo, J.; Gomperts, R.; Stratmann, R. E.; Yazyev, O.; Austin, A. J.; Cammi, R.; Pomelli, C.; Ochterski, J. W.; Ayala, P. Y.; Morokuma, K.; Voth, G. A.; Salvador, P.; Dannenberg, J. J.; Zakrzewski, V. G.; Dapprich, S.; Daniels, A. D.; Strain, M. C.; Farkas, O.; Malick, D. K.; Rabuck, A. D.; Raghavachari, K.; Foresman, J. B.; Ortiz, J. V.; Cui, Q.; Baboul, A. G.; Clifford, S.; Cioslowski, J.; Stefanov, B. B.; Liu, G.; Liashenko, A.; Piskorz, P.; Komaromi, I.; Martin, R. L.; Fox, D. J.; Keith, T.; Al-Laham, M. A.; Peng, C. Y.; Nanayakkara, A.; Challacombe, M.; Gill, P. M. W.; Johnson, B.; Chen, W.; Wong, M. W.; Gonzalez, C.; Pople, J. A. *Gaussian 03*, revision C.02; Gaussian, Inc.: Wallingford, CT, 2004.

(56) Becke, A. D., III. *J. Chem. Phys.* **1993**, *98*, 5648–52.

(57) McLean, A. D.; Chandler, G. S. *J. Chem. Phys.* **1980**, *72*, 5639–48.

(58) Cossi, M.; Barone, V.; Cammi, R.; Tomasi, J. *Chem. Phys. Lett.* **1996**, *255*, 327–335.

(59) Locknar, S. A.; Peteanu, L. A.; Shuai, Z. *J. Phys. Chem. A* **1999**, *103*, 2197–2201.

(60) Cave, R. J.; Burke, K.; Castner, E. W., Jr. *J. Phys. Chem. A* **2002**, *106*, 9294–9305.

(61) Duan, X.-H.; Li, X.-Y.; He, R.-X.; Cheng, X.-M. *J. Chem. Phys.* **2005**, *122*, 084314/1–084314/9.
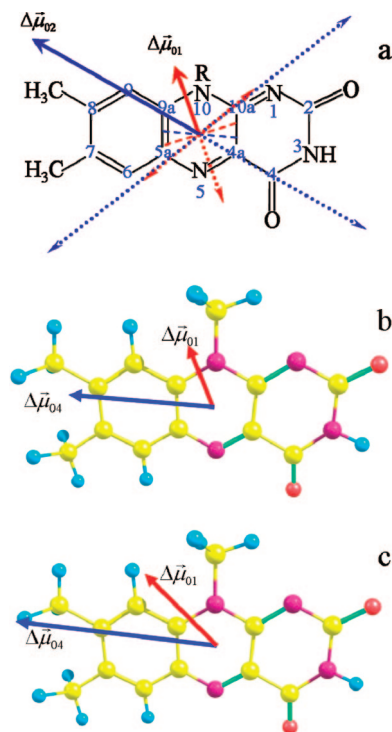
Figure 3. (a) Difference dipole moment vectors for FAD in PL$_{OX}$ based on Stark fitting. Solid arrows are in good agreement with calculated difference dipoles, while dotted arrows represent other vector orientations consistent with the Stark data analysis. The directions of the calculated transition dipole moments are shown as color-coded short dashed lines. (b) Difference dipole moments from TDDFT/finite field calculations for vacuum and (c) CCl$_4$ based on the PCM solvent model.

vibronic band for S$_0$→S$_1$ occurring at approximately 21 186 cm^{-1} (472 nm) and the S$_0$→S$_2$ band occurring at approximately 26 171 cm^{-1} (382 nm). The feature to the red of the lowest energy transition is a small amount of PL$_{SQ}$.

It can be seen that each vibronic band in the S$_0$→S$_1$ transition has been split into two closely spaced peaks (state numbering for the experimental spectra follows the commonly used nomenclature). This has been observed by us previously in the low temperature absorption and Stark spectra of Old Yellow Enzyme,[47] an FMN-binding flavoprotein. The splitting could be due to heterogeneity in the FAD binding site, but, as suggested in our earlier study, it appears more likely that a vibrational degeneracy is being lifted by hydrogen bonding with the protein. This is further corroborated by the observation that only single bands are observed at low temperature for flavins in nonprotic solvents.[46] The S$_0$→S$_2$ band does not show this splitting, but this may be due to the inherently broader line width of this transition. Interestingly, freezing the protein does not induce any significant spectral shifts. This suggests that the FAD binding pocket maintains its structure at low temperature. The peak positions have been tabulated in Table S1. The 77 K spectrum was fitted to two sets of Gaussian functions (see Figure S1), and the parameters from this fit (width, center, and amplitude) were used as a starting point for the simultaneous fitting of the Stark and absorption spectra described below.

The Stark spectra of PL$_{OX}$ at 220 μM for two different polarizations, $\chi = 54°$ and 90°, are presented as averages from several different runs and have been normalized to $F_{ext} = 10^6$ V/cm to reduce noise and facilitate comparison (Figure 2b). The spectra were corrected for concentration, path length, and the refractive index of the buffer. The second derivative nature of

	$|\Delta\vec{\mu}_{0n}|$ (D·f) ($\pm\sigma$)	ζ_A^{0n} (deg) ($\pm\sigma$)	$Tr\Delta\bar{\bar{\alpha}}_{0n}$ Å^3 f^2 ($\pm\sigma$)
PL$_{OX}^{01}$	2.7 (0.3)	55 (3)	134 (13)
PL$_{OX}^{02}$	7.3 (0.5)	35 (7)	57 (26)
PL$_{SQ}^{01}$	3.9 (0.5)	51 (7)	86 (14)
PL$_{SQ}^{02}$	2.9 (0.6)	64 (9)	236 (26)

the signal is apparent, and this enhances the vibronic splitting described above. The spectrum obtained at the magic angle ($\chi = 54°$) is equal in amplitude to the $\chi = 90°$ spectrum for the S$_0$→S$_1$ transition (~20 000−24 000 cm^{-1}, ~500−417 nm). The magic angle Stark spectrum of the S$_0$→S$_2$ transition (~24 500−30 000 cm^{-1}, ~408−333 nm) is significantly larger than its $\chi = 90°$ counterpart. The different dichroic ratios correspond with the linear dichroism (LD) data of Eaton et al. for flavodoxin absorption in single crystals.[62] Fitting these data as described above yields values for $|\Delta\vec{\mu}_{0n}|$, ζ_A^{0n}, and $Tr\Delta\bar{\bar{\alpha}}_{0n}$, where the index for excited states $n = 1, 2, 3,...,$ for the two bands (see Table 1). Excitation of the low energy transition leads to a dipole moment change of $|\Delta\vec{\mu}_{01}| = 2.7 \pm 0.3$ D·f. This difference dipole makes an angle of $\zeta_A^{01} = 55° \pm 3°$ with respect to $\vec{m}_{01}$. The change in polarizability is $Tr\Delta\bar{\bar{\alpha}}_{01} = 134 \pm 13$ Å^3 f^2. For the $\vec{m}_{02}$ transition, the difference dipole increases nearly 3-fold, $|\Delta\vec{\mu}_{02}| = 7.3 \pm 0.5$ D·f, $\zeta_A^{02} = 35° \pm 7°$, and $Tr\Delta\bar{\bar{\alpha}}_{02} = 57 \pm 26$ Å^3 f^2. In both transitions, the difference dipole represents the largest contribution to charge redistribution. These values compare quite well with those obtained for flavins in simple solvents ($\sim|\Delta\vec{\mu}_{01}| = 2.5$ D·f and $|\Delta\vec{\mu}_{02}| = 7.5$ D·f, respectively[45,46]). A more detailed discussion is given below, but a major conclusion from these results is that there is no evidence of charge transfer interactions between the isoalloxazine ring and the protein, including W382, for the two lowest energy transitions.

A knowledge of the transition dipole moment directions for flavin is required to assign the directions of the measured difference dipole moments. In 1975, Eaton et al. measured these $\vec{m}_{0n}$ for both the oxidized and the semiquinone flavin (mono-nucleotide) in flavodoxin single crystals,[62] and these values have guided our study. However, because of the isotropic orientation of the flavin molecules, Stark spectroscopy cannot provide a unique assignment of the direction of the $\Delta\vec{\mu}_{0n}$ in the molecular frame. The experimentally determined angle ζ_A^{0n} only provides the orientation of $\Delta\vec{\mu}_{0n}$ to $\vec{m}_{0n}$, which still leaves an infinite number of vectors that form a double cone about $\vec{m}_{0n}$. As we shall show below, the transition dipoles and difference dipoles from the TDDFT calculations support placing the $\Delta\vec{\mu}_{0n}$ in the plane of the flavin. This limits the set of $\Delta\vec{\mu}_{0n}$ to four for each transition, each of the same magnitude but with different directions such that $\angle\Delta\vec{\mu}_{0n}, \vec{m}_{0n} = \zeta_A^{0n}$. With this assumption, the experimentally derived directions for $\Delta\vec{\mu}_{0n}$, $n = 1,2$ for the two transitions are shown in Figure 3a, where the $\Delta\vec{\mu}_{01}$ is indicated by red arrows and the $\Delta\vec{\mu}_{02}$ are color-coded blue. To assign the difference dipole directions uniquely requires further information. Therefore, we used TDDFT calculations to help narrow the possible $\Delta\vec{\mu}_{0n}$ directions derived from the experimental data.

TDDFT Calculations on Lf$_{OX}$ and the Assignment of the PL$_{OX}$ Stark Spectra. The electronic structures of the S$_0$, S$_1$, and S$_2$ states were calculated using TDDFT. The starting coordinates for Lf$_{OX}$ were obtained from the *A. nidulans* crystal structure

(62) Eaton, W. A.; Hofrichter, J.; Makinen, M. W.; Andersen, R. D.; Ludwig, M. L. *Biochemistry* **1975**, *14*, 2146–2151.

Table 2. Electronic Structure Parameters from TDDFT Calculations[a]

species	f_{osc}	λ_{max} (nm)	μ_n (D)[b]	$\Delta\mu_{0n}$ (D)[c]	ζ_A^{0n} (deg)
Lf_{OX}^{01}/vac	0.20	412.4	11.9	1.8	64
Lf_{OX}^{04}/vac	0.15	326.0	18.3	4.4	11
Lf_{OX}^{01}/CCl$_4$	0.26	423.4		2.3	41
Lf_{OX}^{04}/CCl$_4$	0.26	343.7		6.4	10
Lf_{OX}^{01}/MeOH	0.23	423.6		2.8	30
Lf_{OX}^{03}/MeOH	0.28	348.5		6.8	7
Lf_{SQ}^{01}/vac	0.098	595.8	10.7	1.9	80
Lf_{SQ}^{03}/vac	0.0039	418.2	7.8	1.5	30
Lf_{SQ}^{01}/CCl$_4$	0.13	581.0		2.3	69
Lf_{SQ}^{02}/CCl$_4$	0.013	446.9		1.2	20
Lf_{SQ}^{03}/CCl$_4$	0.060	436.2		4.6	16
Lf_{SQ}^{01}/MeOH	0.12	567.8		2.6	59
Lf_{SQ}^{02}/MeOH	0.017	451.9		2.0	3
Lf_{SQ}^{03}/MeOH	0.066	441.5		4.6	11

[a] Only transitions to states with $f_{osc} > 0.001$ are included. [b] From Rho-CI density calculations.[61] [c] From finite-field calculations.

Table 3. DFT-Calculated Ground-State Dipole Moments as a Function of Solvent

species	μ_0 (D)
Lf_{OX}/vacuum	9.8
Lf_{OX}/CCl$_4$	12.3
Lf_{OX}/MeOH	13.3
Lf_{SQ}/vacuum	9.8
Lf_{SQ}/CCl$_4$	12.7
Lf_{SQ}/MeOH	13.7

of Mees et al.[9] where a methyl group was substituted at N_{10} and hydrogens were added as necessary. Optimization from these coordinates yielded a planar geometry (see Figure S10 for bond lengths and axis system). This supports the simplifying assumption that the $\Delta\vec{\mu}_{0n}$ reside in the flavin plane. Calculations of the transition dipole moment directions for the two lowest energy bright transitions agree well with the experimentally derived directions from Eaton et al.[62] These vectors, shown in Figure 3a, are positioned $+17°$ and $-5°$ relative to the long axis of the flavin for $\vec{m}_{01}$ and $\vec{m}_{04}$, respectively, as compared to $+15°$ and $-5°$ from Eaton's measurements (positive angle is counterclockwise relative to the long axis). TDDFT calculations were performed to account for the change in electronic properties due to solvent, using a polarizable continuum model (PCM). The permanent ground-state dipole moments, $\vec{\mu}_0$, for Lf_{OX} were 9.8, 12.7, and 13.3 D in vacuum, CCl$_4$, and MeOH, respectively (Table 3). The increase in the dipole moment in the polar solvents is to be expected, given that the dipole moment is roughly parallel to the cavity electric field. TDDFT calculations returned transition energies and dipole moments (see Table 2), as well as the x, y, and z components of the transition dipole moments (see Table S2). The calculated oscillator strengths for LF$_{OX}$ in vacuum were obtained for the $S_0 \rightarrow S_1$ ($f_{osc} = 0.20$) and $S_0 \rightarrow S_4$ ($f_{osc} = 0.15$) transitions, with $\lambda_{max} = 412$ nm and $\lambda_{max} = 326$ nm, respectively (both $\vec{m}_{02}$ and $\vec{m}_{03}$ had near zero f_{osc}). The calculated wavelength maxima were about 60 nm to the blue of the protein maxima (about 3062 and 4504 cm^{-1} for $\vec{m}_{01}$ and $\vec{m}_{04}$, respectively). For a dielectric of about 5 (CCl$_4$), the band maxima red-shifted, giving $\lambda_{max} = 423$ nm and $\lambda_{max} = 344$ nm for the wavelength maxima of $\vec{m}_{01}$ and $\vec{m}_{04}$, respectively (both $\vec{m}_{02}$ and $\vec{m}_{03}$ had near zero f_{osc}), in much closer agreement with the experimental result. Interestingly, calculations using methanol as a dielectric ($n \approx 33$) did not significantly change the transition energies, but did lead to a reordering of MOs such that the bright transitions were now $\vec{m}_{01}$ ($\lambda_{max} = 423$ nm) and $\vec{m}_{03}$ ($\lambda_{max} = 344$ nm). This points to the critical role played by

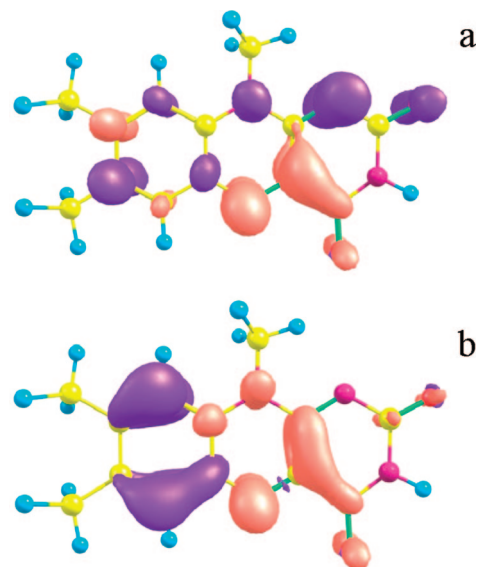**Figure 4.** (a) Difference electron density of the $S_0 \rightarrow S_1$ transition calculated for Lf_{OX} in vacuum. Purple indicates positive charge, while red indicates negative charge. (b) Difference electron density of the $S_0 \rightarrow S_2$ transition.

the solvent cavity electric field, which is addressed more fully in the discussion of the semiquinone results.

Finite-field calculations were used to obtain the difference dipole moment magnitudes and directions. The magnitudes of $\Delta\vec{\mu}_{0n}$ and their directions relative to the corresponding transition dipole moment, ζ_A^{0n}, are given in Table 2. The calculated $\Delta\vec{\mu}_{0n}$ lie approximately in the plane of the flavin (Figure 3b,c for vacuum and CCl$_4$, respectively), which itself is planar in this oxidation state. In fact, the z component of the permanent dipole moments from the Rho-CI calculations was usually much less than 0.1% of the magnitude of the x or y components (see Tables S4,S5).

The ratio of $|\Delta\vec{\mu}_{02}|/|\Delta\vec{\mu}_{01}|$ is about 2.4 for both vacuum and MeOH, and about 2.8 for CCl$_4$, all of which are within 10% of the experimental ratio for the protein (2.7). This agreement provides a basis for the use of the excited-state calculations in narrowing down the Stark assignments.

The directions of the $\Delta\vec{\mu}_{0n}$ did not vary much with the dielectric constant and justify the refinement of the experimental assignments. Overall, the calculations agree quite well with the experimental $\Delta\vec{\mu}_{0n}$ indicated by the solid arrows in Figure 3a. These are the same $\Delta\vec{\mu}_{0n}$ that were found in our previous work on the electronic structure of flavins in simple solvents,[46] on OYE,[47] and from our work on the substrate electrochromism hypothesis.[63]

The difference electron densities for the two transitions (vacuum) are shown in Figure 4a,b. Calculations performed using a PCM solvent model did not differ from the vacuum results significantly. Electron-rich regions of the molecule are colored red, and electron-deficient regions are colored purple. Electron density is highest along the $N_5-C_{4a}-C_{10}$ portion of the molecule for both transitions. The xylene ring is net electron deficient for both transitions, while the pyrimidine ring shows a net excess of electron density. The significance of this result is discussed below in the context of photoreduction of PL$_{OX}$.

Low Temperature Absorption and Stark Spectra of PL$_{SQ}$. The absorption spectrum of PL$_{SQ}$ in glycerol/buffer A (2:1 v:v) frozen glass is compared to its room temperature absorption

(63) MacFarlane, A. W., IV; Stanley, R. J. *Biochemistry* **2001**, *40*, 15203–15214.
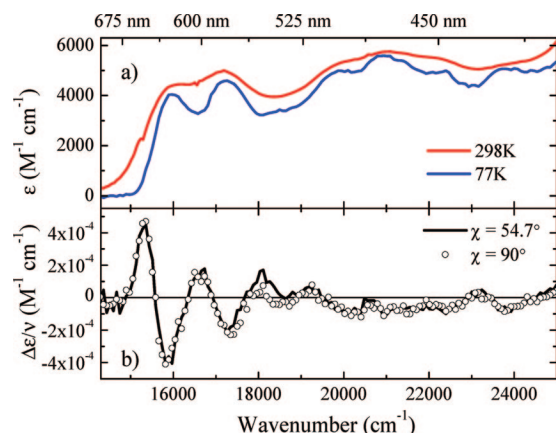
ARTICLES

Figure 5. (a) Room temperature (red line, 1.3 mM) and 77 K (blue line, 8 μM) absorption spectra of PL$_{SQ}$. (b) Energy-weighted Stark spectra of 330 μM PL$_{SQ}$ taken at $\chi = 54°$ (−) and 90° (○) and normalized to 1 MV/ cm. The symbol used to plot the 90° data is sized to appropriately reflect the magnitude of the standard deviation from the mean for the averaged scans.

spectrum under the same conditions as shown in Figure 5a. To our knowledge, this is the first report of a low temperature absorption spectrum of PL$_{SQ}$ or, for that matter, any flavoprotein semiquinone. The room temperature spectrum was obtained on a 1.3 mM PL$_{SQ}$ sample in a conventional 1 mm quartz cuvette and UV/vis spectrometer (1 s integration time/1 scan), while the 77 K spectrum was obtained using our COWS spectrometer at a concentration of 8 μM (5.8 cm path length) with about the same total acquisition time (100 ms time constant/9 scans). The slightly lower signal-to-noise ratio of the COWS-derived spectrum is probably due to scattering of the frozen glass in the 5.8 cm path length of the waveguide. Nonetheless, the quality is comparable to the 298 K spectrum even though the protein concentration is less than 1/150th of the room temperature sample. The near overlap of the spectra suggests that aggregation effects in the 298 K sample are negligible at this level of analysis.

At both temperatures, the absorption spectrum of FADH• in photolyase shows two overlapping visible transitions, $D_0 \rightarrow D_1$ (15 385−18 018 cm^{-1}, ~650−555 nm) and $D_0 \rightarrow D_2$ (~19 050−24 390 cm^{-1}, ~525−410 nm). These two transitions were also identified by Eaton et al. in their single crystal linear dichroism studies of semiquinone flavodoxin.[62] Vibronic resolution is more pronounced at low temperature and shows that the conformational space available to the FADH• is restricted at 77 K. This spectral signature also strongly suggests that freezing the protein does not lead to cold denaturation, as a free flavosemiquinone would be extremely sensitive to oxidation. As further confirmation, we have observed that frozen solutions of PL$_{SQ}$ (and PL$_{RED}$, unpublished observation) maintain their oxidation state upon warming to room temperature. As with PL$_{OX}$, no temperature-dependent spectral shifts were evident, and the measured peak positions were within a few nanometers of the room temperature assignments of Schelvis' laboratory[64] (Table S1). Two sets of Gaussian functions were fitted to the 77 K absorption spectrum for the $D_0 \rightarrow D_1$ and $D_0 \rightarrow D_2$ transitions to allow for an analysis of the Stark spectra (Figure S2).

The Stark spectra of 330 μM PL$_{SQ}$ in glycerol/buffer (2:1 v:v) frozen glasses at two different probe polarizations are shown

in Figure 5b. The average of four spectra was normalized to 1 MV/cm first after correcting for concentration, path length, and the refractive index of the buffer. As in the case of PL$_{OX}$, second derivatives of the absorption spectrum contribute prominently to the Stark spectrum, suggesting that the $\Delta\vec{\mu}_{0n}$ dominates the change in electronic structure. The low energy transition, $D_0 \rightarrow D_1$, is more prominent than the $D_0 \rightarrow D_2$ transition. This may be attributed, in part, to the more highly resolved vibronic structure of the low energy transition. The band spacing of this progression is larger than that for the high energy transition, an observation corroborated by Schelvis.[64] The greater congestion for the high energy band can easily cause cancelation of the second derivatives associated with each vibronic band, as has been observed in other systems.[65] This can be seen more clearly in an example of a fit of the energy-weighted Stark spectrum to sums of zeroth, first, and second derivatives of absorption spectra, as shown in Figure S3.

Eaton et al. considered that the molecular orbitals of oxidized and semiquinone flavin[62] were identical but that only the occupancy changed depending on which oxidation state was considered. This appears to be corroborated by our measurements, as the changes in electronic structure measured for the semiquinone are in the same range as for PL$_{OX}$. For the $D_0 \rightarrow D_1$ transition, $|\Delta\vec{\mu}_{01}| = 3.9 \pm 0.5$ D•f and $\zeta_A^{01} = 51° \pm 7°$ with respect to $\hat{m}_{01}$. The change in the mean polarizability is $Tr\Delta\bar{\bar{\alpha}}_{01} = 86 \pm 14$ Å$^3 f^2$. For the $D_0 \rightarrow D_2$ transition, $|\Delta\vec{\mu}_{02}| = 2.9 \pm 0.6$ D•f and $\zeta_A^{02} = 64° \pm 9°$. The change in the mean polarizability for this transition is $Tr\Delta\bar{\bar{\alpha}}_{02} = 236 \pm 26$ Å$^3 f^2$. The contributions of each of these components to the fit of the Stark spectrum can be seen in Figure S3. Interestingly, the change in the magnitude of the difference dipole moments and polarizabilities between the two lowest energy bright transitions in PL$_{SQ}$ is reversed as compared to PL$_{OX}$ (e.g., $\Delta\vec{\mu}_{01}^{OX} < \Delta\vec{\mu}_{02}^{OX}$, but $\Delta\vec{\mu}_{01}^{SQ} > \Delta\vec{\mu}_{02}^{SQ}$). This has consequences for interpreting solvatochromism in flavosemiquinones. Contrary to the argument made above for a lack of charge transfer in PL$_{OX}$, we have nothing with which to compare the semiquinone protein Stark spectrum, so any statement about charge transfer involving FADH• for these transitions would be premature.

The ζ_A^{0n} values afford a mapping of the difference dipoles onto the molecular framework as shown in Figure 6a. Using the aforementioned simplification, there are four possible sets of vectors for each transition (eight total, red→$\Delta\vec{\mu}_{01}$, blue→$\Delta\vec{\mu}_{02}$). The two vectors shown as solid arrows give the best agreement with the TDDFT calculations, as discussed below.

TDDFT Calculations of Lf$_{SQ}$ and the Assignment of the PL$_{SQ}$ Stark Spectra. To our knowledge, this is the first time TDDFT has been used to probe the excited-state electronic structure of the flavin neutral radical. The ground-state dipole moment of semiquinone lumiflavin and the transition dipole moment directions for the two lowest energy bright transitions in vacuum were calculated using TDDFT at the UB3LYP/6-311+G (d,p) level. Optimization of the radical starting from the crystal structure coordinates (pdb code 1TEZ) yielded a planar geometry for FADH•. This is different from the initial geometry taken from the experimental crystal structure of Mees,[9] which shows a ~9° "butterfly" bend. They ascribe this geometry to fully reduced FAD (i.e., FADH$^-$). Interestingly, the flavin is planar in all other PL crystal structures from *E. coli*,[5] *T.*

(64) Schelvis, J. P. M.; Ramsey, M.; Sokolova, O.; Tavares, C.; Cecala, C.; Connell, K.; Wagner, S.; Gindt, Y. M. *J. Phys. Chem. B* **2003**, *107*, 12352−12362.

(65) Silverman, L. N.; Spry, D. B.; Boxer, S. G.; Fayer, M. D. *J. Phys. Chem. A* **2008**, *112*, 10244−10249.
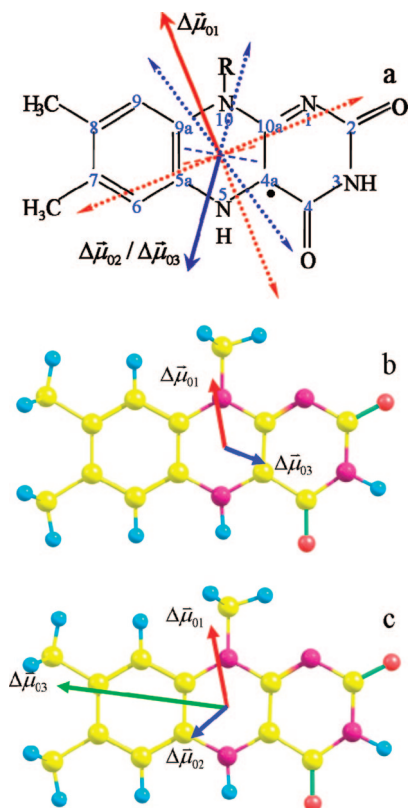
Figure 6. (a) Difference dipole moment vectors for FADH[•] in PL$_{SQ}$ based on Stark fitting. The solid arrows are in good agreement with the calculated difference dipoles, while the dotted arrows represent other vector orientations consistent with the data analysis. The directions of the calculated transition dipole moments are shown as color-coded short dashed lines. (b) Difference dipole moments for Lf$_{SQ}$ from TDDFT/finite field calculations in vacuum and (c) CCl$_4$ based on the PCM solvent model.

thermophilus,[66,67] *S. tokodaii*,[20] *A. thaliana* (Cry-DASH[30]), and an earlier one from *A. nidulans*.[19] Our computed geometry suggests that these latter crystal structures are reporting on semiquinone (or possibly oxidized, see above) photolyase. Fortuitously, the computed planar geometry affords a simplification of the assignment of the difference dipoles (see Figure S11 for bond lengths and axis system).

The excitation energies are in good agreement with the experimental absorption spectrum of FADH[•] for DNA photolyase. The lowest energy electronic transition, $D_0 \rightarrow D_1$, was calculated to have $\lambda_{max} = 590.83$ nm and $f_{osc} = 0.098$ for the corresponding experimental band found at 580−620 nm. The $D_0 \rightarrow D_2$ transition had zero oscillator strength. The next bright state, $D_0 \rightarrow D_3$, had an oscillator strength of $f_{osc} = 0.0039$, and the wavelength of this transition was $\lambda_{max} = 440.6$ nm. This corresponds to the experimentally observed broad 400−530 nm band. However, the experimental absorption spectrum shows almost equal intensity for the two bright transitions. This discrepancy might be due to the influence of the surrounding protein environment. The calculated transition dipole moment directions for the $D_0 \rightarrow D_1$ and $D_0 \rightarrow D_3$ transitions were +14° and −10° relative to the long axis of the flavin, respectively, as compared to +16° and −7° from the LD measurements, in

(66) Komori, H.; Masui, R.; Kuramitsu, S.; Yokoyama, S.; Shibata, T.; Inoue, Y.; Miki, K. *Proc. Natl. Acad. Sci. U.S.A.* **2002**, *98*, 13560–5.

(67) Klar, T.; Kaiser, G.; Hennecke, U.; Carell, T.; Batschauer, A.; Essen, L.-O. *ChemBioChem* **2006**, *7*, 1798–1806.

excellent agreement with the experimentally determined transition dipole moment directions from linear dichroism studies[62] on FMNH[•] in flavodoxin single crystals (see Tables S2 and S3).

Difference dipole moments for Lf$_{SQ}$ in vacuum were calculated using the finite field method as described above and are plotted on the flavin molecular framework in Figure 6b. The values for the $D_0 \rightarrow D_1$ and $D_0 \rightarrow D_3$ transitions are 1.9 and 1.5 D, respectively. Without an estimate of the local field correction, f, it is not surprising that the experimental result of 3.9 D·f and 2.9 D·f differs from the calculated values. However, the ratio $|\Delta\vec{\mu}_{03}|/|\Delta\vec{\mu}_{01}| \approx 1.27$ from the calculation should be comparable to $|\Delta\vec{\mu}_{02}|/|\Delta\vec{\mu}_{01}| \approx 1.34$ from the Stark fit. These ratios differ by about 6%, suggesting that TDDFT, using the UB3LYP/6-311+G (d,p) basis set, provides a reasonable measure of the magnitude of charge redistribution for the electronic structure of the radical.

The $\hat{m}_{0n}$ directions from the TDDFT calculations (Table S3) provide some guidance in choosing the appropriate experimental $\Delta\vec{\mu}_{0n}$ vector that most closely matches it. The calculated direction of $\Delta\vec{\mu}_{01}$ is independent of the choice of solvent. The experimental $\Delta\vec{\mu}_{01}$ that most closely matches these three calculations is indicated as a solid red arrow in Figure 6a. The agreement is quite good, with the Stark result differing less than 10° from the TDDFT prediction. The calculated vacuum $\Delta\vec{\mu}_{03}$ vector supports the Stark-derived difference dipole that points toward the C_4 carbonyl oxygen (dotted blue arrow). However, calculations done using CCl$_4$ and MeOH suggest an alternative assignment for higher excited states to the vacuum case.

The inclusion of a polar solvent in the calculations complicates the interpretation for the higher energy transition and stands in stark contrast to the Lf$_{OX}$ case where there was no significant change in calculated electronic structure as a function of solvent dielectric. These results are summarized in Table S2. The lowest energy transition in CCl$_4$ and MeOH red shifts to $\lambda_{max} = 581.0$ nm and $\lambda_{max} = 567.8$ nm, respectively, with essentially equivalent f_{osc}, in excellent agreement with the experimental spectrum. However, both solvent calculations introduce a new state with non-negligible oscillator strength, such that two transitions essentially overlap to form the experimentally assigned $D_0 \rightarrow D_2$ band. The calculated f_{osc} for the $D_0 \rightarrow D_2$ and $D_0 \rightarrow D_3$ transitions are 0.013 and 0.060 for CCl$_4$, and 0.0017 and 0.066 for MeOH. The transition energies for the two bands in either solvent are within 10 nm of each other, centered at about $\lambda_{max} = 440$ nm for CCl$_4$ and $\lambda_{max} = 446$ nm for MeOH. The spectra for these transitions would overlap under our experimental conditions. In addition, the calculated ζ_A^{0n} values are within 8°, suggesting that the dichroic Stark measurements would not resolve these bands either.

The difference dipole moments for these three transitions were calculated using the finite field method and are shown in Figure 6c for the CCl$_4$ case. Interestingly, both the $\Delta\vec{\mu}_{02}$ and the $\Delta\vec{\mu}_{03}$ vectors have rotated nearly 150° in the plane of the flavin relative to the vacuum case. The near overlap of the calculated $D_0 \rightarrow D_2$ and $D_0 \rightarrow D_3$ transitions suggests that the analysis of the experimental Stark spectrum may not be straightforward. A linear combination of the two calculated difference dipole moments suggests that the closest match to the experiment is the difference dipole pointing nearly at N_5 (solid blue arrow, Figure 6a), but that this is really a mixture of the two transitions. The ratio of $(\Delta\vec{\mu}_{03}^{calc}/\Delta\vec{\mu}_{02}^{calc})^2 \approx 15$, suggesting that the Stark spectrum should be dominated by the $D_0 \rightarrow D_3$ transition almost entirely based on the difference dipole alone. In addition, $f_{osc}^{03}/f_{osc}^{02} \approx 4$, again suggesting that the Stark spectrum would report on only the higher energy transition. If this is the case, then the
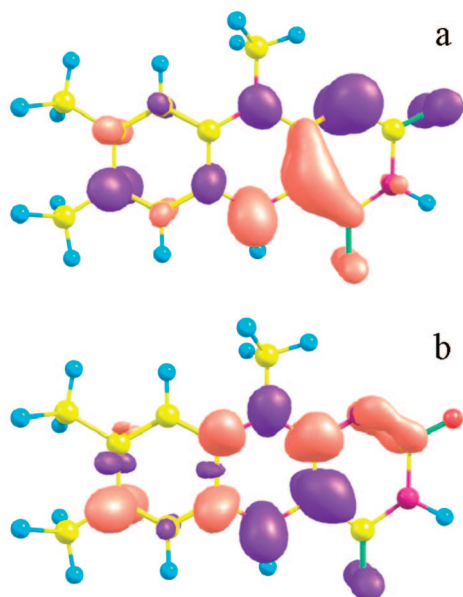
Figure 7. (a) Difference electron density of the $D_0 \rightarrow D_1$ transition calculated for Lf_{SQ} in vacuum. Purple color indicates positive charge, while red indicates negative charge. (b) Difference electron density of the $D_0 \rightarrow D_3$ transition.

ratio of the calculated $\Delta\vec{\mu}_{01}/\Delta\vec{\mu}_{03} \approx 0.5-0.6$, whereas the experimental ratio, $|\Delta\vec{\mu}_{01}|/|\Delta\vec{\mu}_{02}|$, is ~1.3. However, the sensitivity of the calculated values of $|\Delta\vec{\mu}_{0n}|$ for $n > 1$ and f_{osc} on the dielectric constant is not insignificant, as opposed to what was observed for Lf_{OX}, and may point to limitations in TDDFT to calculate accurate properties for higher excited states of radicals of large organic molecules.

Difference electron density maps for vacuum and for CCl_4 and MeOH solvents were calculated to visualize the extent of charge redistribution upon excitation. The difference density was essentially the same in the two solvents, but these differed from the vacuum case for the $D_0 \rightarrow D_3$, as was observed for the directions of the difference dipoles described above (again, the calculated $D_0 \rightarrow D_2$ transition is omitted because of its low oscillator strength and smaller $\Delta\mu$). Because both solvents produced essentially the same result, we discuss only the CCl_4 case and present these difference density maps for the two transitions in Figure S12.

For both vacuum and solvent cases, these maps show that the charge redistribution for the $D_0 \rightarrow D_1$ transition is characterized by excess electron density near the $N_5 - C_{4a}$ region, and an electron-deficient region that spans the $N_{10} - N_1 - C_2$ region and the $C_{5a} - C_7$ region (Figures 7a, S12a). This latter result has important implications for the photoreduction of $*FADH^{\bullet}$ by W382, as discussed below.

For vacuum, the charge redistribution for the $D_0 \rightarrow D_3$ transition is nearly the inverse of the lowest energy transition density (Figure 7b), with excess electron density spread throughout the $C_{5a} - C_7$ and $N_{10} - N_1 - C_2$ regions. Inclusion of solvent changes this result however (see Figure S12b), making the xylene moiety highly electron-deficient. However, in both cases, the D_3 state should decay rapidly through internal conversion to D_1, according to Kasha's rule. Thus, electron transfer from W382 → $*FADH^{\bullet}$ should occur through the D_1 state of the flavosemi-

quinone, making the charge distribution of this state that which is sensed by the W382 donor in the photoreduction process.

Discussion

Stark spectroscopy provides a unique window into the degree and direction of charge displacement upon photoexcitation.[54,65,68−71] While our work represents the first application of Stark spectroscopy to light-driven flavoproteins, others have used this approach to study other photobiological systems such as photosystem II,[70,72,73] light harvesting arrays,[71,74] carotenoids,[75,76] photoactive yellow protein,[77] retinal,[78,79] and the bacterial reaction center.[54,80−85]

Our Stark data are of high quality, but their interpretation is not without difficulty. A precise knowledge of the transition dipole moment directions of the molecule is required. For oxidized and semiquinone flavin, these were available from LD studies of FMN in single crystals as cited above and were confirmed here by TDDFT calculations.

Even with this critical information, there are several further confounding factors. While the transition dipole moment is indeed a vector, the magnitude of the observed Stark effect depends on the vector (dot) product of $\vec{m}_{0n}$ with the direction of the oscillating electric field of the probe light. This, along with the isotropic orientation of the sample, only allows for the specification of the direction of charge displacement in terms of a double cone of vectors at an angle ζ_A^{0n} (for $\Delta\vec{\mu}_{0n}$). While the planarity of the flavin in both oxidized and semiquinone forms reduces the ambiguity significantly, there are still four possible directions of $\Delta\vec{\mu}_{0n}$ that are consistent with the data analysis.

In this study, we have used TDDFT with a large basis set to help guide our assignments. However, it must be acknowledged that TDDFT has been shown to incorrectly evaluate charge transition contributions, albeit most seriously for intermolecular CT.[86] Despite this limitation, the TDDFT/finite field calculations

(68) Peteanu, L.; Locknar, S. *Chem. Phys. Lett.* **1997**, *274*, 79−84.
(69) Karki, L.; Vance, F. W.; Hupp, J. T.; LeCours, S. M.; Therien, M. J. *J. Am. Chem. Soc.* **1998**, *120*, 2606−2611.
(70) Yanagi, K.; Hashimoto, H.; Gardiner, A. T.; Cogdell, R. J. *J. Phys. Chem. B* **2004**, *108*, 10334−10339.
(71) Premvardhan, L.; Sandberg, D. J.; Fey, H.; Birge, R. R.; Buechel, C.; van Grondelle, R. *J. Phys. Chem. B* **2008**, *112*, 11838−11853.
(72) Olszowka, D.; Krawczyk, S.; Maksymiec, W. *Biochim. Biophys. Acta: Bioenergetics* **2004**, *1657*, 61−70.
(73) Losche, M.; Feher, G.; Okamura, M. Y. *NATO Sci. Ser., Ser. A* **1988**, *149*, 151−64.
(74) Somsen, O. J. G.; Chernyak, V.; Frese, R. N.; Van Grondelle, R.; Mukamel, S. *J. Phys. Chem. B* **1998**, *102*, 8893−8908.
(75) Premvardhan, L.; Papagiannakis, E.; Hiller, R. G.; van Grondelle, R. *J. Phys. Chem. B* **2005**, *109*, 15589−15597.
(76) Krawczyk, S.; Britton, G. *Biochim. Biophys. Acta: Protein Struct. Mol. Enzymol.* **2001**, *1544*, 301−310.
(77) Premvardhan, L. L.; van der Horst, M. A.; Hellingwerf, K. J.; van Grondelle, R. *Biophys. J.* **2003**, *84*, 3226−3239.
(78) Mathies, R.; Stryer, L. *Proc. Natl. Acad. Sci. U.S.A.* **1976**, *73*, 2169−2173.
(79) Locknar, S. A.; Peteanu, L. A. *J. Phys. Chem. B* **1998**, *102*, 4240−4246.
(80) Lösche, M.; Feher, G.; Okamura, M. Y. *Proc. Natl. Acad. Sci. U.S.A.* **1987**, *84*, 7537−7541.
(81) Lockhart, D. J.; Boxer, S. G. *Biochemistry* **1987**, *26*, 664−8.
(82) Lockhart, D. J.; Boxer, S. G. *Chem. Phys. Lett.* **1988**, *144*, 243−50.
(83) Lockhart, D. J.; Boxer, S. G. *Proc. Natl. Acad. Sci. U.S.A.* **1988**, *85*, 107−11.
(84) Middendorf, T. R.; Mazzola, L. T.; Lao, K.; Steffen, M. A.; Boxer, S. G. *Biochim. Biophys. Acta* **1993**, *1143*, 223−34.
(85) Moser, C. C.; Sension, R. J.; Szarka, A. Z.; Repinec, S. T.; Hochstrasser, R. M.; Dutton, P. L. *Chem. Phys.* **1995**, *197*, 343−354.
(86) Dreuw, A.; Head-Gordon, M. *Chem. Rev.* **2005**, *105*, 4009−4037.

of the difference dipole moments for oxidized lumiflavin provide very good agreement with one set of experimentally derived $\Delta\mu$ values and were useful in supporting a unique assignment. This was independent of the dielectric constant used. However, the magnitude of the $\Delta\vec{\mu}_{0n}$ depends significantly on the computational approach and basis set.

Consider a recent multireference configuration interaction (MRCI) calculation of ground and excited-state oxidized flavin dipole moments.[87] MRCI should be capable of high accuracy, but the computational results show poor agreement with time-resolved microwave conductivity and solvatochromism,[88] and Stark spectroscopic values[45−47] for the excited-state and difference dipole moments. A DFT/MRCI study by Neiss et al.[89] was in closer agreement with our experimental results for PL_{OX} and the calculations for Lf_{OX}, with $\Delta\vec{\mu}_{01} \approx 1$ D as compared to 1.8 D, and $\Delta\vec{\mu}_{02} \approx 5$ D as compared to 4.4 D for this study. Similar results were obtained for 10-methylisoalloxazine by Salzmann et al. using the same method.[90] A recent TDDFT study, using the aug-cc-pVDZ basis and B3YLP functional, gave much the same difference electron density for the $S_0 \rightarrow S_1$ transition in Lf_{OX}.[91] An SAC-CI study on Lf_{OX} gave comparable ground and excited-state dipole moments[92] to our study. Wolf et al.[93] used CIS to obtain $\Delta\mu_{01} \approx 1$ D, in agreement with the (similar) calculation of Neiss. Unfortunately, none of these studies report on the directions of the permanent dipole moments, so the difference dipoles cited therein are the maximum possible.

The application of TDDFT to obtain unique assignments of the Stark spectrum of PL_{SQ} is not nearly as unambiguous. Several other groups have used computational methods to study the semiquinone, but only in its ground state.[94−96] These studies all predict that the ground state will be planar. Our TDDFT calculations also gave a planar structure.

Again, the inclusion of a PCM dielectric did not appreciably change the lowest energy transition (this is an important conclusion as discussed below), but the solvent electric field has a profound effect on the ordering of the MOs. This, in turn, changes the nature of the allowed transitions, moving an $n \rightarrow \pi^*$ transition too high in energy to be relevant, and lowering the energy of a $\pi \rightarrow \pi^*$ transition sufficiently to make it the primary contribution to the absorption spectrum. A definitive determination of the direction of charge displacement for the (experimental) $D_0 \rightarrow D_2$ transition is not available from our analysis.
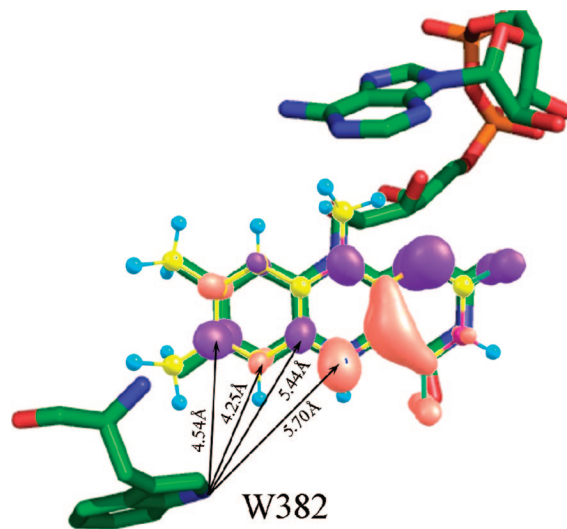
(87) Climent, T.; Gonzalez-Luque, R.; Merchan, M.; Serrano-Andres, L. *J. Phys. Chem. A* **2006**, *110*, 13584–13590.

(88) Shcherbatska, N. V.; Bastiaens, P. I. H.; Visser, A. J. W. G.; Jonker, S. A.; Warman, J. M. In *Dipole Moments in the Ground and Excited State of Flavin from Molecular Relaxation Spectroscopy and Microwave Conductivity*; Time-Resolved Laser Spectroscopy in Biochemistry III; Lakowicz, J. R., Ed.; 1992; pp 180−190.

(89) Neiss, C.; Saalfrank, P.; Parac, M.; Grimme, S. *J. Phys. Chem. A* **2003**, *107*, 140–147.

(90) Salzmann, S.; Tatchen, J.; Marian, C. M. *J. Photochem. Photobiol., A: Chem.* **2008**, *198*, 221–231.

(91) Yoong-Kee Choe, S. N. K. N. *J. Comput. Chem.* **2007**, *28*, 727–739.

(92) Hasegawa, J.-Y.; Bureekaew, S.; Nakatsuji, H. *J. Photochem. Photobiol., A: Chem.* **2007**, *189*, 205–210.

(93) Wolf, M. M. N.; Schumann, C.; Gross, R.; Domratcheva, T.; Diller, R. *J. Phys. Chem. B* **2008**, *112*, 13424–13432.

(94) Weber, S.; Moebius, K.; Richter, G.; Kay, C. W. M. *J. Am. Chem. Soc.* **2001**, *123*, 3790–3798.

(95) Zheng, Y.-J.; Ornstein, R. L. *J. Am. Chem. Soc.* **1996**, *118*, 9402–9408.

(96) Garcia, J. I.; Medina, M.; Sancho, J.; Alonso, P. J.; Gomez-Moreno, C.; Mayoral, J. A.; Martinez, J. I. *J. Phys. Chem. A* **2002**, *106*, 4729–4735.

Figure 8. FADH• and W382 in the active site of *E. coli* photolyase (1DNP), showing the spatial and electronic structure relationship between the flavin cofactor and the Trp donor. The orange regions are electron rich, while the purple regions represent electropositive regions of the molecule.

Finally, it is important to point out that our experimental and computational difference dipole moments obtained for FADH• support the analysis of Murphy et al.[97] in which they measured spectroscopic shifts in PL_{SQ} upon binding of a cytidine dimer substrate molecule. In that study, they assumed that the difference dipole moment of FADH• for the lowest energy transition was about the same as that for FAD_{OX}. Here, we have shown that these difference dipoles differ by about 40% (Table 1), justifying their assumption. In turn, the analysis of the spectral shift in FADH• by Murphy et al. supports our measurement for $|\Delta\vec{\mu}_{01}| \approx 4$ D for the $D_0 \rightarrow D_1$ transition in FADH•.

Charge Redistribution in PL_{SQ}: Physiological Significance. We discuss the PL_{SQ} results first, as the semiquinone is an intermediate in DNA repair and is the electron acceptor in the photoreduction or photoreactivation of photolyase. However, the significance of our findings bears directly on the blue light photoreception mechanism of cryptochrome[29,98] as photoinduced electron transfer is at work in both PL_{SQ} photoreduction and cryptochrome signaling.

The donor is a nearby tryptophan residue (W382 in *E. coli* PL), and the acceptor is *FADH•. If we assume Kasha's Rule is operative, then excitation of either $\vec{m}_{0n}$, $n = 1-2$, will lead to relaxation to the D_1 state with the net result that electron transfer involves this state. The relative orientation of W382 to the excited (D_1) FADH• is therefore critical for efficient electron transfer. In fact, W382 is just underneath this part of the xylene ring, which is consistent with the experimental $\Delta\vec{\mu}_{01}$ having its positive component pointing in the direction of the xylene moiety (Figure 6a). Not surprisingly, ground-state DFT calculations show that the Trp N_1 atom is electron-rich (data not shown). A more subtle picture of the differential charge distribution from the TDDFT results (Figure 7a) shows that both the xylene and the pyrimidine rings have electropositive patches in the D_1 state. The $C_{10a}-N_1$ locus on the pyrimidine moiety is sterically blocked by the ribityl-adenosine portion of the FAD (Figure 8), making the placement of a proximal Trp untenable.

(97) Murphy, A. K.; Tammaro, M.; Cortazar, F.; Gindt, Y. M.; Schelvis, J. P. M. *J. Phys. Chem. B* **2008**, *112*, 15217–15226.

(98) Ozturk, N.; Song, S.-H.; Selby, C. P.; Sancar, A. *J. Biol. Chem.* **2008**, *283*, 3256–3263.

It is conceivable that a Trp residue placed close to the $C_2=O$ of the flavin could be a competitive initial electron donor for photoreduction, but this polar side of the flavin is preferentially solvated by polar or charged residues (Ser238, Asp372) or by the ribose, whose $2'$-OH group is within 4 Å of the carbonyl. The other electropositive patch on the $C_{5a}-C_7$ part of the xylene ring is in a relatively hydrophobic region. The distances between the Trp N_1 atom and flavin N_5, C_{5a}, C_6, and C_7 atoms are indicated in Figure 8. Based on a $\beta = 1.0$ Å^{-1} for the electronic coupling term ($\alpha e^{-\beta r}$), the ratio of the electronic coupling between the Trp N_1 to the flavin sites above shows that the relative rate constants decrease by a factor of 3 for transfer to the flavin N_5 and modestly increase by about 30% for the C_6 site, relative to transfer to C_7. These are not large differences, so we believe that electrostatics dominates which electron transfer pathway[99] is most likely, that is, Trp $N_1 \rightarrow$ Flavin C_7. Balancing the lowest Coulombic barrier with the shortest distance for electron transfer is consistent with the C_7 atom being the site of photoreduction by Trp382. Therefore, our results rationalize, and post facto predict, the location of Trp382 with respect to the flavin ring.

Is the Electronic Structure of FAD in PL$_{OX}$ Unique? The Stark spectrum for oxidized flavin has been published by us previously. In one set of studies, we explored the two lowest excited states in FMN, FAD, and N3-methyl-7,8-dimethylisoalloxazine, in frozen glasses of glycerol:water,[45] ethanol, butanol, and 2-MTHF.[46] More recently, we analyzed the Stark spectrum of FMN in OYE$_{OX}$.[47] The $|\Delta\vec{\mu}_{0n}|$ and ζ_A^{0n} were identical within experimental error for these diverse environments. The trend in the $Tr\Delta\bar{\bar{\alpha}}_{0n}$ was different for PL$_{OX}$ than either the simple flavin or the OYE$_{OX}$ cases, with the difference mean polarizability for $n = 1$ being larger in PL$_{OX}$ than $n = 2$. This difference may reflect the different local environments of the flavin in each case, particularly if hydrogen-bonding patterns differ. In this case, electron density from solvent may be donated or removed from the flavin ring via the nitrogen and carbonyl oxygen atoms, respectively. In the simple solvent studies, alcohols and 2-MTHF were used, all of which can hydrogen bond with the N_3 hydrogen atom of the flavin ring. 2-MTHF, however, is incapable of acting as a hydrogen-bond donor. However, we cannot, at this time, make a comparison of the $Tr\Delta\bar{\bar{\alpha}}_{0n}$ values to a flavin in a non-hydrogen bonding solvent (e.g., toluene). Such a study would be useful in understanding how hydrogen bonding to flavin affects its polarizability change upon excitation and might be particularly valuable in ascertaining the role of hydrogen bonding in altering the electronic structure (e.g., reduction potential) of flavins in flavoproteins generally.

The magnitude, if not the direction, of the difference dipole moments in simple solvents was corroborated by Isoda et al., who used Stark spectroscopy to study flavin oriented in Langmuir–Blodgett (L–B) films.[100] Their use of an oriented sample should provide an unambiguous determination of the angle between $\Delta\vec{\mu}_{0n}$ and the applied field. They found that $\Delta\vec{\mu}_{0n}$ ($n = 1, 2$) were collinear and pointed toward C_6, in contrast to our findings in this and previous reports. It may be the case that the protein matrix shifts the direction of $\Delta\vec{\mu}_{0n}$ as compared to the L–B film, but our studies on FMN in OYE[47] gave $\Delta\vec{\mu}_{0n}$ that were not significantly different from those obtained in simple solvents. This is further confirmed in this study by the

TDDFT calculations as a function of dielectric constant. Another difference between our work and that of Isoda et al. is that no analysis of polarizability changes was undertaken by Isoda, despite a non-negligible $Tr\Delta\bar{\bar{\alpha}}_{0n}$ obtained in our studies for $n = 1, 2$. Finally, Isoda et al. performed their work at room temperature. It may be that the orientation achieved in the L.B. film was scrambled due to polling of the flavin molecules under the influence of the 700 Hz, 7.6×10^5 V/cm applied electric field. This effect must be taken into account, given the large ground-state dipole moment of the molecule. The use of frozen glasses in our studies has the advantage that molecules are unable to reorient to the external field to any significant degree.

Most recently, however, Weigel et al. have measured the dynamic solvation shift for the $S_0 \rightarrow S_1$ transition of oxidized riboflavin (RF) in water and DMSO.[101] They estimated that a dipole moment change in the range of $\Delta\bar{\mu}_{01} = 3-6$ D is necessary to explain the $500-1000$ cm^{-1} solvation shift. To provide for this result, it was necessary to invoke dynamic mixing of the $^1n\pi^*$ state into the $^1\pi\pi^*$ state, resulting in a larger $\Delta\bar{\mu}_{01}$ than is expected by steady-state spectroscopy. However, our results (assuming $f = 1.3$) show that the dipole moment change is not more than 2 debye. This suggests that the $S_0 \rightarrow S_1$ transition is more purely $\pi \rightarrow \pi^*$ in the Franck–Condon region.

Taken together, our Stark spectroscopy studies seem to suggest that the electronic interaction between the oxidized flavin and the solvent (protein) does not produce a measurable perturbation to the electronic structure of the cofactor, except where charge transfer from excited states of the flavin as the acceptor is significant.[47]

Charge Redistribution in PL$_{OX}$: Physiological Significance. The photoreduction of PL$_{OX}$ has not been thought to be a physiological process, and the mechanism has not been studied in great detail. However, it has become apparent that the oxidized form of the cryptochrome protein is photobiologically significant.[33,98,102,103] Thus, the charge redistribution that takes place upon photoexcitation of FAD$_{OX}$ in PL can give important information about Cry. We recount what is known about PL$_{OX}$ photochemistry first to place our results in the proper context.

We start with the flavin chromophore excited-state dynamics. In 2000, we published time-resolved two color pump–probe studies of FMN and FAD in water and formamide solvents.[104] Excitation was performed from 385 to 412 nm to selectively excite (as much as possible within experimental constraints) the $S_0 \rightarrow S_2$ and $S_0 \rightarrow S_1$ transitions. The single wavelength probe was tuned from 393 to 650 nm. The cross correlation for these experiments was about 175 fs. Our results showed that internal conversion from $S_2 \rightarrow S_1$ occurred in less than 100 fs. Following this process, S_1 vibrational relaxation was observed to take place in less than 500 fs. A 5 ps component was assigned to quenching of the singlet excited flavin by adenine (for FAD) or by exogenous purines.

In 2001, we published the first transient absorption spectrum of E. coli PL$_{OX}$.[63] Excitation was achieved using 200 fs pulses centered at 400 nm, and a white light continuum was used to

(99) Prytkova, T. R.; Beratan, D. N.; Skourtis, S. S. *Proc. Natl. Acad. Sci. U.S.A.* **2007**, *104*, 802–807.

(100) Suzuki, S.; Isoda, S.; Maeda, M. *Jpn. J. Appl. Phys., Part 1* **1989**, *28*, 1673–6.

(101) Weigel, A.; Dobryakov, A. L.; Veiga, M.; Perez Lustres, J. L. *J. Phys. Chem.*, ACS ASAP.

(102) Hoang, N.; Schleicher, E.; Kacprzak, S.; Bouly, J.-P.; Picot, M.; Wu, W.; Berndt, A.; Wolf, E.; Bittl, R.; Ahmad, M. *PLoS Biol.* **2008**, *6*, 1811.

(103) Banerjee, R.; Schleicher, E.; Meier, S.; Viana, R. M.; Pokorny, R.; Ahmad, M.; Bittl, R.; Batschauer, A. *J. Biol. Chem.* **2007**, *282*, 14916–14922.

(104) Stanley, R. J.; MacFarlane, A. W., IV. *J. Phys. Chem. A* **2000**, *104*, 6899–6906.

probe the spectral evolution of *PL$_{OX}$ from 410−650 nm. Based on a truncated time window, a single exponential component of ca. 30 ps was fitted to the decay of the excited state. However, a new broadband feature was observed above 550 nm, giving evidence for a charge transfer (CT) intermediate formed within picoseconds of excitation of FAD$_{OX}$. The CT band persisted for many nanoseconds. Our conclusion was that the CT donor involved either the FAD adenine or a nearby aromatic amino acid residue (probably Trp).

Recently, several new time-resolved studies of PL$_{OX}$ have appeared. In 2005, Gauden et al.[105] made femtosecond transient absorption measurements on AppA, a flavoprotein that senses blue light. They observed that internal conversion from S$_2$→S$_1$ occurred in 170 fs, followed by vibrational relaxation in about 1.6 ps. We consider these results to corroborate our own,[104] given the difference in solvation between simple solvents and a protein. Schleicher's group performed nanosecond transient absorption spectroscopy of PL$_{OX}$ in an external magnetic field to test whether the PL radical formed by this photoreduction reaction might be sensitive to magnetic field effects.[106] They found that PL$_{OX}$ undergoes photoreduction to the semiquinone anion (FAD$^{•-}$) but does not continue to PL$_{SQ}$, confirming our earlier observation of charge transfer in excited-state PL$_{OX}$.[63] Zhong's group reported a similar finding using femtosecond spectroscopy with excitation at 400 nm and a single wavelength 710 nm probe beam.[107] They observed two components within the time window of our earlier experiment, a 1.8 ps component assigned to *FAD→FAD$^{•-}$ decay and a 54 ps component assigned to formation of W382$^+$. It has long been known that both the S$_0$→S$_1$ and the S$_0$→S$_2$ transitions are excited at 400 nm with roughly equal probability.[62,108] Therefore, it is possible and even likely that the 1.8 ps component represents ultrafast internal conversion from S$_2$→S$_1$ as well as relaxation dynamics,[101] suggesting that the time constant for the FAD$^{•-}$ process may be the observed 54 ps component, more in line with our analysis.

What is the significance of the current study with regard to the role of tryptophan in PL$_{OX}$ photoreduction? If Kasha's rule is operative (excited higher states decay rapidly to the lowest excited state), then our work suggests that the same Trp residues used to reduce the semiquinone also act as electron donors to the photoexcited oxidized FAD, because the S$_1$ state develops the same electropositive patch in the vicinity of C$_7$ as D$_1$ in FADH$^•$ (compare Figures 4a and 7a). It appears fortuitous that the oxidized and semiquinone forms have $\Delta\vec{\mu}_{0n}$ that point roughly in the same direction. Had this not been the case, and if PL$_{OX}$ was physiologically relevant, then perhaps a second set of Trp residues would have been incorporated into PL for this process to be efficient. However, Eaton et al.[62] showed that both Fl$_{OX}$ and FlH$_{SQ}$ can be considered to have the same orbital or electronic structure and that only the occupation of these orbitals differentiates the two oxidation states. Our results

suggest this to be the case, at least qualitatively if not quantitatively.

Concluding Remarks

Looking beyond photolyase, the light-driven blue light flavophotoreceptors all operate from the excited state, whether singlet oxidized (e.g., BLUF and LOV domains) or doublet semiquinone. In the case of the LOV domains, an excited-state singlet→triplet intersystem crossing occurs to produce a flavin C$_{4a}$−S−Cys covalent adduct that initiates signaling.[39,40] This reaction may involve a zwitterionic (charge transfer) state that could be accessed sensitively using Stark spectroscopy.

The X-ray crystallographic structures of BLUF domains TePixD,[109] SyPixD,[110] AppA,[111,112] and BlrB[113] have been recently reported. In these proteins, a conserved tyrosine residue in the vicinity of the flavin replaces the tryptophan found in photolyases and cryptochromes. Mutagenesis studies showed that this tyrosine is essential for its function.[114] Recent time-resolved studies by Gauden et al. showed transient intermediates in the photoreaction of SyPixD are a FAD radical anion (FAD$^{•-}$) and the subsequently formed neutral radical (FADH$^•$).[115] They proposed that the nearby tyrosine is oxidized by the excited-state singlet state of flavin (FAD*) with subsequent formation of a Tyr$^•$−FADH$^•$ radical pair. The tyrosine is positioned close to the flavin xylene ring at about 4 Å, suggesting that electron transfer occurs from tyrosine through the C$_6$−C$_7$ part of the xylene ring in the flavin. Thus, BLUF proteins appear to share the same photoreduction pathway as photolyases, but for different mechanistic ends. In AppA, there is a semiconserved tryptophan present within 4 Å proximal to the flavin O$_4$ atom. Mutagenesis studies by Gauden et al.[115] showed that this particular tryptophan is not a good electron donor to FAD*, suggesting that the positioning of the aromatic donor residue relative to the flavin xylene ring is crucial for efficient electron transfer and catalytic activity.

In conclusion, the tools we have developed will provide insight into whether charge transfer is involved in a wide variety of light-driven flavoproteins. For example, future Stark spectroscopy/computational chemistry studies of cryptochromes may address why they are difficult to reduce beyond the semiquinone.[98,103] This attribute may be connected with the interaction of a conserved asparagine residue (in both Cry-DASH and PL) that hovers over N$_5$. Whether this change in the excited-state electronic structure of the flavin caused by this interaction can be quantified by Stark spectroscopy is a challenge we face.

(105) Gauden, M.; Yeremenko, S.; Laan, W.; van Stokkum, I. H. M.; Ihalainen, J. A.; Van Grondelle, R.; Hellingwerf, K. J.; Kennis, J. T. M. *Biochemistry* **2005**, *44*, 3653–3662.
(106) Henbest, K. B.; Maeda, K.; Hore, P. J.; Joshi, M.; Bacher, A.; Bittl, R.; Weber, S.; Timmel, C. R.; Schleicher, E. *Proc. Natl. Acad. Sci. U.S.A.* **2008**, *105*, 14395–14399.
(107) Kao, Y.-T.; Tan, C.; Song, S.-H.; Oztuerk, N.; Li, J.; Wang, L.; Sancar, A.; Zhong, D. *J. Am. Chem. Soc.* **2008**, *130*, 7695–7701.
(108) Sun, M.; Moore, T. A.; Song, P.-S. *J. Am. Chem. Soc.* **1972**, *94*, 1730–1740.
(109) Kita, A.; Okajima, K.; Morimoto, Y.; Ikeuchi, M.; Miki, K. *J. Mol. Biol.* **2005**, *349*, 1–9.
(110) Yuan, H.; Anderson, S.; Masuda, S.; Dragnea, V.; Moffat, K.; Bauer, C. *Biochemistry* **2006**, *45*, 12687–12694.
(111) Anderson, S.; Dragnea, V.; Masuda, S.; Ybe, J.; Moffat, K.; Bauer, C. *Biochemistry* **2005**, *44*, 7998–8005.
(112) Jung, A.; Reinstein, J.; Domratcheva, T.; Shoeman, R. L.; Schlichting, I. *J. Mol. Biol.* **2006**, *362*, 717–732.
(113) Jung, A.; Domratcheva, T.; Tarutina, M.; Wu, Q.; Ko, W.-h.; Shoeman, R. L.; Gomelsky, M.; Gardner, K. H.; Schlichting, I. *Proc. Natl. Acad. Sci. U.S.A.* **2005**, *102*, 12350–12355.
(114) Kraft, B. J.; Masuda, S.; Kikuchi, J.; Dragnea, V.; Tollin, G.; Zaleski, J. M.; Bauer, C. E. *Biochemistry* **2003**, *42*, 6726–6734.
(115) Gauden, M.; Grinstead, J. S.; Laan, W.; van Stokkum, I. H. M.; Avila-Perez, M.; Toh, K. C.; Boelens, R.; Kaptein, R.; Van Grondelle, R.; Hellingwerf, K. J.; Kennis, J. T. M. *Biochemistry* **2007**, *46*, 7405–7415.

Supporting Information Available: PL absorption and Stark spectra with fits; derivative spectra from the Stark fit; tables of peak positions of spectra (PL_{SQ}); transition dipole moment components and oscillator strengths; and computed spectra. Optimized geometries of PL_{OX} and PL_{SQ} are given, with bond lengths and reference x, y, and z axes. This material is available free of charge via the Internet at http://pubs.acs.org.

JA809214R